Spin-relaxation times exceeding seconds for color centers with strong spin-orbit coupling in SiC

Maia Gilardoni, Carmem; Bosma, Tom; Hien, Danny van; Hendriks, Freddie; Magnusson, Björn; Ellison, Alexandre; Ivanov, Ivan G.; Son, N. T.; Wal, Caspar H. van der

Published in:
New Journal of Physics

DOI:
10.1088/1367-2630/abbf23

Publication date:
2020

New Journal of Physics
The open access journal at the forefront of physics

Deutsche Physikalische Gesellschaft DPG IOP Institute of Physics

PAPER • OPEN ACCESS

Spin-relaxation times exceeding seconds for color centers with strong spin–orbit coupling in SiC

To cite this article: Carmem M Gilardoni *et al* 2020 *New J. Phys.* **22** 103051

New Journal of Physics
The open access journal at the forefront of physics

Deutsche Physikalische Gesellschaft DPG
IOP Institute of Physics

Published in partnership with: Deutsche Physikalische Gesellschaft and the Institute of Physics

OPEN ACCESS

RECEIVED
8 July 2020

REVISED
22 September 2020

ACCEPTED FOR PUBLICATION
7 October 2020

PUBLISHED
26 October 2020

PAPER

Spin-relaxation times exceeding seconds for color centers with strong spin–orbit coupling in SiC

Carmem M Gilardoni[1,4,*], Tom Bosma[1,4], Danny van Hien[1], Freddie Hendriks[1], Björn Magnusson[2], Alexandre Ellison[2], Ivan G Ivanov[3], N T Son[3] and Caspar H van der Wal[1]

[1] Zernike Institute for Advanced Materials, University of Groningen, NL-9747AG Groningen, The Netherlands
[2] Norstel AB, Ramshällsvägen 15, SE-602 38 Norrköping, Sweden
[3] Department of Physics, Chemistry and Biology, Linköping University, SE-581 83 Linköping, Sweden
[*] Author to whom any correspondence should be addressed.
[4] These authors contributed equally to this work.

E-mail: c.maia.gilardoni@rug.nl

Keywords: semiconductor defects, quantum information, defect symmetries, spin–lattice interaction

Supplementary material for this article is available online

Abstract

Spin-active color centers in solids show good performance for quantum technologies. Several transition-metal defects in SiC offer compatibility with telecom and semiconductor industries. However, whether their strong spin–orbit coupling degrades their spin lifetimes is not clear. We show that a combination of a crystal-field with axial symmetry and spin–orbit coupling leads to a suppression of spin–lattice and spin–spin interactions, resulting in remarkably slow spin relaxation. Our optical measurements on an ensemble of Mo impurities in SiC show a spin lifetime T_1 of 2.4 s at 2 K.

1. Introduction

Spin-active color centers in semiconductors have attracted significant interest for the implementation of quantum technologies, since several of these systems combine long-lived spin states with a bright optical interface [1–4]. Long distance spin entanglement has been achieved for a variety of defects as stationary nodes [5–8]. However, finding suitable emitters that combine long-lived spins, short excited-state lifetimes and optical transitions compatible with telecommunication fiber-optic infrastructure in an industrially established material has remained elusive. Silicon carbide, a wide band-gap semiconductor with mature fabrication technology, hosts a range of defect centers with optical transitions near or at the telecom range [9, 10], including several defects containing transition metal (TM) impurities [11–17]. The electronic and spin properties of these defects derive largely from the character of the d-orbitals of the TM under the action of a crystal field determined by the lattice site [18–20]. Furthermore, the presence of a heavy atom in the defect implies that spin–orbit coupling (SOC) plays a significant role in the electronic structure of these color centers. Generally, as widely demonstrated by the solid state spin–qubit community, combining favorable spin properties and strong SOC can be challenging [17, 21–23].

We report here on slow spin relaxation with T_1 exceeding seconds below 4 K for a molybdenum defect ensemble in 6H–SiC, indicating that the defect spin is surprisingly robust with respect to spin relaxation despite the presence of strong SOC. In order to understand this, we measure the spin-relaxation time of the Mo defect in SiC between 2 and 7 K and identify the main processes leading to spin relaxation in this temperature range. We analyze the manifestation strength of these processes, while considering the electronic structure of the defect, and find that a combination of axial rotational symmetry and SOC suppresses several spin-relaxation mechanisms in this system, leading to unexpectedly long T_1. The analysis leading to these conclusions is general, relying on the character of the d-orbitals of the TM and the particular symmetry of the defect. Thus, a similar approach could be relevant in the interpretation of

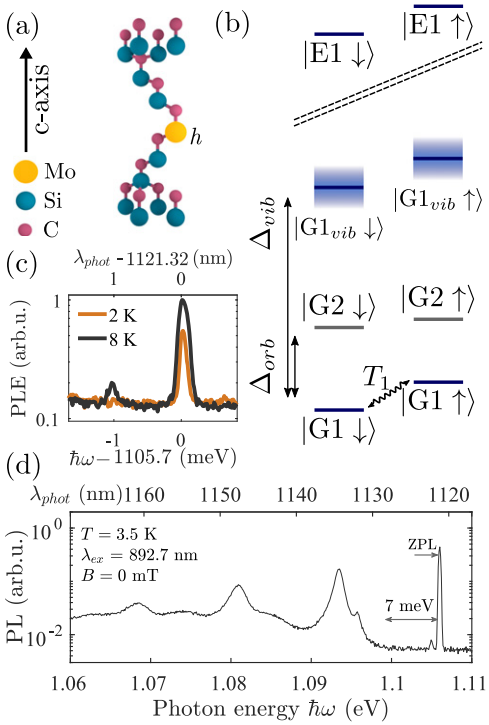

Figure 1. Defect and electronic structure. (a) The defect is composed of a Mo atom positively ionized substituting a Si at a quasi-hexagonal (*h*) lattice site. (b) Both ground ($|G1\rangle$) and optically excited ($|E1\rangle$) states are characterized by a spin doublet which is split by a magnetic field. Additionally, a second ground-state Kramer's doublet ($|G2\rangle$) is present approximately 1 meV above the ground state doublet. (c) When this second doublet is thermally occupied, a second ZPL appears in the PLE spectrum, where the light emitted in the phonon sideband is measured as a function of the laser photon energy $\hbar\omega$. (d) The electronic ground state can couple to localized vibrational modes, giving rise to vibronic states $|G1_{vib}\rangle$, as evidenced by the phonon replicas observed in the PL spectrum.

experiments on other point defects in crystals with analogous symmetries, such as vanadium defects in SiC (with optical transitions compatible with telecom infrastructure), group IV defects in diamond and point-defects in transition metal dichalcogenides [14, 16, 18, 24–26].

2. Methods

We focus on the Mo defect associated with an optical transition line at 1121.3 nm in 6H–SiC, which consists of a Mo impurity in a Si substitutional site of quasi-hexagonal symmetry (figure 1(a), *h* site) [13, 15]. The defect is positively ionized, such that after binding to four neighboring carbons, the TM is left with one active unpaired electron in its 4-d shell. In this lattice site—and only considering the rotational symmetry of the defect—both ground and excited states are two-fold orbitally degenerate, such that the orbital angular momentum is not quenched [20]. In the presence of SOC, the orbital degeneracy is broken, giving rise to two Kramer's doublets (KD) in the ground and two KDs in the excited state (figure 1(b)) [13, 15], resembling what is observed for the group IV defects in diamond [25].

Each KD is a doublet composed of a time-reversal pair: the doublet splits as an effective spin-1/2 system in the presence of a magnetic field, but its degeneracy is otherwise protected by time-reversal symmetry (see [27, section IV]). The energy difference between the two spin–orbit split KDs in the ground state, Δ_{orb} in figure 1(b), is expected to be approximately 1 meV [15], in accordance with the appearance of a second zero-phonon line (ZPL) in resonant photoluminescence excitation (PLE) experiments at approximately 8 K (figure 1(c)). Finally, the presence of sharp phonon replicas of the ZPL in the photoluminescence spectrum indicates that the defect center couples strongly to localized vibrational modes (figure 1(b) and (d)).

We measure the spin-relaxation time of this defect by means of a pump–probe experiment as shown in figure 2. Experiments are performed on an esemble of defects in a 6H–SiC sample previously investigated in reference [13]. The sample showed p-doped character, and the defect concentration was estimated to be between 10^{14} and 10^{16} cm^{-3}. We create pulses out of a CW laser beam by using a combination of an electro-optical phase modulator (EOM) and a Fabry–Pérot (FP) cavity. The EOM generates sidebands from our CW laser at frequency steps determined by an RF input signal; by tuning the FP cavity to transmit this sideband only, we create pulses that turn on/off as the RF generator turns on/off. These pulses resonantly

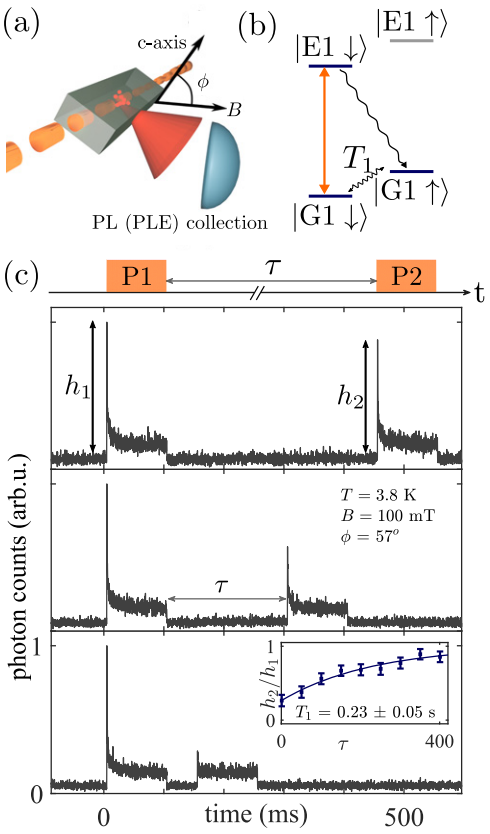

Figure 2. Time-resolved hole burning experiment. (a) In order to investigate T_1, we perform time-resolved pump-probe experiments where we resonantly excite the sample in the presence of a magnetic field and collect the phonon-sideband emission. (b) When the magnetic field is non-collinear with the symmetry axis of the defect, spin–flipping transitions between ground and optically excited states are allowed. (c) The first pulse P1 probes the population at thermal equilibrium in the ground-state spin sublevel $|G1\downarrow\rangle$ (which we call bright state in this work, since it can be optically excited), and polarizes the spin population into a spin sublevel that cannot be optically excited, $|G1\uparrow\rangle$ (which we here call dark state). After a variable delay τ, a second pulse P2 probes the recovery of the population in the bright state. (Inset) The ratio of the leading-edge peaks in the PLE signal (h_2/h_1) recovers monoexponentially as a function of the delay between the two pulses.

drive optical transitions between ground and excited states, and we measure the photon emission into the phonon sideband with a single-photon counter after filtering out the laser line. We apply a magnetic field non-collinear with the *c*-axis of the sample such that spin–flipping transitions between ground and optically excited states are allowed (figure 2(a) and (b)) [13]. In order to counteract slow ionization of the defects (see [27, section III] for further details), we apply a repump laser in between measurements [13, 28–30].

3. Results

In the pump–probe experiment (figure 2(c)), the initial response of the sample to pulse P1, h_1, provides a measure of the population in the bright spin state $|G1\downarrow\rangle$ at thermal equilibrium (see the caption of figure 2 for an explanation of the terms dark and bright spin sublevels in this work). The sharp increase (decrease) of the PL signal as the pulse turns on (off) indicates that both the optical decay rate and the Rabi frequency are relatively fast (see [27, section V] for further details). Optical excitation provided by P1 polarizes the spin ensemble in a dark spin sublevel ($|G1\uparrow\rangle$ in figure 2(b)) within the first few microseconds, as evidenced by the decrease and subsequent saturation of the PLE signal (the saturation level shows that the effective T_1 is lower when the laser is on, see [27, section V]). The leading-edge response of the ensemble to a second (probe) pulse P2, h_2, reflects the recovery of the population in the bright spin sublevel ($|G1\downarrow\rangle$ in figure 2(b)) during the time τ between the two optical pulses. Between 2 K and 7 K, we observe a monoexponential recovery of h_2 towards h_1 as a function of τ (figure 2(d)), which must correspond to the spin-relaxation time T_1 given the considerations presented below.

We repeat this experiment at zero magnetic field in order to confirm that the PL darkening observed within the first few microseconds of optical excitation corresponds to optical pumping of the ensemble into a dark spin sublevel. In this case, we observe no leading-edge peak in the PLE signal, indicating that no

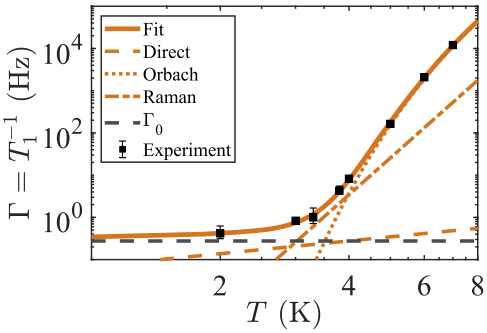

Figure 3. Temperature dependence of spin relaxation. The variation of $\Gamma = T_1^{-1}$ with temperature can be accurately described by a combination of direct (one-phonon), Raman and Orbach processes (two-phonon processes). The two-phonon processes happen due to coupling to an excited state approximately 6.5 meV above the ground state KD, compatible with coupling of the electronic state of the defect to localized vibrational modes. Error bars are extracted from the exponential fits of the data presented in the inset of figure 2(c) (for details, see [27, section VII]), and are smaller than the data points when not visible.

optical pumping occurs at this timescale if the spin sublevels are degenerate [27, figure S2] (https://stacks.iop.org/NJP/22/103051/mmedia). The absence of PL darkening at zero magnetic field implies that we cannot trap Mo centers in state $|G2\rangle$ for observable times. This is the case if the optical decay rate between states $|E1\rangle$ and $|G2\rangle$ is smaller than the relaxation rate between the two ground state KDs $|G1\rangle$ and $|G2\rangle$ in the temperature range investigated. (We expect the optical decay rate between $|E1\rangle$ and $|G2\rangle$ to be small, since we observe no lines corresponding to this transition in PL and PLE scans). Thus, we conclude that after optical pumping in the presence of a magnetic field, no significant population is trapped in state $|G2\rangle$, and that relaxation dynamics via this level do not affect the signals used to derive T_1. Furthermore, we investigate the timescale associated with bleaching due to ionization [29, 30], which is found to be several orders of magnitude slower than the one associated with spin dynamics [27, section III].

The temperature dependence of the spin-relaxation time spans several orders of magnitude, going from 2.4 s at 2 K to 83 μs at 7 K (figure 3). Concerning phonon mediated spin relaxation, the mechanisms leading to spin relaxation are well established [20, 31]. One (direct) and two-phonon (Raman, Orbach) processes are relevant when transitions between the levels involved are thermally accessible. Direct spin–flip processes are expected to lead to spin-relaxation rates ($\Gamma = T_1^{-1}$) that grow linearly with temperature ($\Gamma_{\text{direct}} \propto T$). In contrast, two-phonon processes mediated by an excited state give rise to spin-relaxation rates that grow superlinearly with temperature ($\Gamma_{\text{Raman}} \propto T^{5<n<11}$ and $\Gamma_{\text{Orbach}} \propto e^{-\Delta/k_B T}$, where Δ is the energy of the relevant excited state) [20, 31–33]. Additionally, interaction with paramagnetic moments in the material is expected to lead to temperature-independent spin relaxation. We fit the data presented in figure 3 to a combination of these processes and identify the temperature regimes where they are relevant (see [27, section VII] for additional details concerning the fitting procedure).

The defect has a rich electronic structure, with orbital and vibrational degrees of freedom at energies that are thermally accessible between 2 and 7 K (figure 1(b)). Thus, we expect two-phonon processes involving transitions into both orbital and vibrational excited states to contribute to the temperature dependence of Γ. Surprisingly, we find that not all available states contribute significantly to spin relaxation, leading to unexpectedly long spin lifetimes below 4 K.

Above 4 K, we identify an exponential growth of Γ as a function of temperature, indicating the prevalence of spin relaxation via Orbach processes in this temperature range. From the fit presented in figure 3, we extract $\Delta = 6.5 \pm 1$ meV for the energy of the excited state involved in these spin flips. This energy matches the difference observed in PL experiments between the ZPL and the onset of the phonon-sideband emission (figure 1(d)). The first phonon replica is observed 10 meV above the ZPL, but its broadened line indicates that the first available vibrational levels are lower in energy. Thus, we identify vibronic levels where the spin is coupled to localized vibrational modes as the relevant excited state for two-phonon mediated spin-relaxation processes that degrade T_1 above 4 K. As expected, these spin-relaxation mechanisms do not depend on the magnitude of the magnetic field [27].

We note that we cannot observe Orbach processes involving states $|G2\rangle$. Between 2 and 7 K, the contribution of these processes to the spin relaxation is expected to be close to saturation, giving a flat temperature dependence in this range. Thus, the long spin-relaxation times observed at 2 K provide an upper bound to the spin-relaxation rates due to two-phonon processes mediated by $|G2\rangle$, and are evidence that these processes are slow. This leads us to conclude that transitions between $|G1\rangle$ and $|G2\rangle$ are strongly spin-conserving. Based on this, we can estimate the timescale of phonon-induced transitions between the two doublets $|G1\rangle$ and $|G2\rangle$ to be on the order of milliseconds [27, 34]. This process is orders of magnitude

slower than the same process in SnV in diamond, a group IV defect with similar mass to the Mo defect in SiC, [26, 35]. We note that, for this class of defects in diamond, the active electrons participate in bonding to the neighboring carbon atoms [25], which may change the character of the phonons responsible for spin–lattice interactions. In fact, the gap observed between the ZPL and the PSB for the Mo defect is absent in the photoluminescence (PL) spectrum of group IV defects in diamond [36], indicating that the latter are more sensitive to low-energy phonons.

Spin-conserving phonon mediated transitions between the two orbital states are expected to contribute to decoherence [37], limiting the spin coherence time T_2 of the $|\mathrm{G1}\rangle$ spin to millisecond timescales at 4 K. This is significantly larger than the experimentally observed ensemble T_2^* [13], likely due to an inhomogeneous distribution of Zeeman splittings [18].

Below 4 K, the slow spin-relaxation rates observed must result from three mechanisms: (i) processes whose temperature dependence is saturated in this range (as treated above); (ii) direct one-phonon transitions between the two spin sublevels $|\mathrm{G1}\downarrow\rangle$ and $|\mathrm{G1}\uparrow\rangle$ and (iii) temperature independent processes (such as spin–spin paramagnetic coupling). The long T_1 observed below 4 K is evidence that all three processes are relatively slow for this particular system. The first contribution has been discussed above. Below, we elaborate on how the electronic structure of this defect leads to a suppression of the latter two processes.

The two spin-sublevels pertaining to a KD are strictly time-reversal symmetric with respect to each other, such that they must be degenerate eigenstates of any external field that preserves time-reversal symmetry. Thus, to first order, phonons or electric fields cannot cause a direct spin–flip within pure KD pairs (but note that this does not concern transitions between levels belonging to different KDs, see [27, section IV]). A magnetic field or the interaction with nearby nuclear spins leads to mixing between spin sublevels pertaining to different KDs, enabling direct spin–flips via interactions with single phonons. This mixing is inversely proportional to the energy separation between the various KDs, which is in turn largely determined by the spin–orbit splitting. Thus, large SOC protects the KD character of the ground state spin doublet, suppressing direct spin–flipping processes within the spin doublet.

Additionally, SOC leads to a highly anisotropic Zeeman splitting of the ground-state spin sublevels [13, 27], which hinders its interaction with a bath of paramagnetic impurities in the SiC crystal. Firstly, the spins are insensitive to magnetic fields perpendicular to their quantization axis, such that small fluctuations in the local magnetic field are not likely to induce a spin flip. Secondly, the spin doublet has a Zeeman splitting governed by a g factor that is at maximum 1.6 [13], suppressing resonant spin flip–flop interactions with neighboring paramagnetic impurities with $g \approx 2$.

The same arguments presented above to explain the long spin-relaxation times observed in this defect indicate that obtaining control of the defect spin via microwave fields is a challenge. Driving spin resonances between the two ground state spin sublevels requires mixing of the various KDs by a perturbation that breaks time-reversal symmetry, such as a strong magnetic field [27, section III]. This is necessary to control the ground state spin via microwaves, and is expected to contribute to spin-relaxation mechanisms.

4. Discussion and conclusion

As discussed above, in the particular case of a TM at a quasi-hexagonal site, such as the Mo center, a combination of rotational symmetry and strong SOC protects the effective spin from flipping: it gives rise to ground state effective spin which is an isolated KD, protected by time-reversal symmetry and magnetically isolated from other paramagnetic centers in the crystal due to its unique Zeeman structure. In this doublet, the crystal field locks the orbital angular momentum along the axis of rotational symmetry of the defect. Via the strong SOC, the electronic spin is stabilized, giving rise to robust effective spin states with long spin-relaxation times.

Considering these processes alone, stronger SOC is thus expected to lead to slower spin-relaxation rates in TM color centers with an odd number of electrons and rotational symmetry. Nonetheless, our work shows that the presence of localized vibrational modes is pivotal in generating spin–flips, their energy determining the temperature where the onset of two-phonon relaxation mechanisms happens. Since the energy and density of states of the localized vibrational modes depend non-trivially on the mass of the defect, whether or not defects containing heavier TMs (where SOC is more prevalent) will exhibit longer spin-relaxation times remains a question. In fact, the class of group IV defects in diamond show significantly faster spin relaxation, which depends non-trivially on the mass of the defect [26, 35]. Thus, it would be relevant to investigate these processes in defects containing 5-d electrons in SiC. Tungsten defects, for example, have been observed with an optical transition at 1240 nm and an odd number of electrons, although their microscopic configuration is still unknown [38].

More generally, SOC should not be regarded as a detrimental feature when investigating solid-state defects for quantum communication applications. Transition metal defects in SiC offer interesting opportunities, such as charge-state switching [39, 40], emission in the near-infrared [14] and long spin lifetimes [17]. The maturity of the SiC-semiconductor industry means that a wide range of defects has been identified [18]. Nonetheless, their characterization with respect to optical and spin properties is still vastly unexplored.

Acknowledgments

We thank A Gali, A Csóré and P Wolff for discussions. Technical support from H de Vries, J G Holstein, T J Schouten, and H Adema is highly appreciated. Financial support was provided by the Zernike Institute BIS program, the EU H2020 project QuanTELCO (862721), the Swedish Research Council grants VR 2016-04068 and VR 2016-05362, the Knut and Alice Wallenberg Foundation (KAW 2018.0071), and the Carl Tryggers Stiftelse för Vetenskaplig Forskning grant CTS 15:339.

Author contributions

The project was initiated by CHvdW and TB. SiC materials were grown and prepared by AE and BM Experiments were performed by TB, DvH and CG, except for the PL measurements which were done by IGI. Data analysis was performed by CG, TB, DvH, FH and CHW. CG, TB, and CHW had the lead on writing the paper, and CG and TB are co-first author. All authors read and commented on the manuscript.

ORCID iDs

Carmem M Gilardoni https://orcid.org/0000-0001-5318-3363
Tom Bosma https://orcid.org/0000-0002-7627-4011
Freddie Hendriks https://orcid.org/0000-0003-4623-7524
Björn Magnusson https://orcid.org/0000-0003-1618-170X
Ivan G Ivanov https://orcid.org/0000-0003-1000-0437
N T Son https://orcid.org/0000-0002-6810-4282
Caspar H van der Wal https://orcid.org/0000-0002-9843-3220

References

[1] Weber J R, Koehl W F, Varley J B, Janotti A, Buckley B B, Van de Walle C G and Awschalom D D 2010 Quantum computing with defects *Proc. Natl Acad. Sci.* **107** 8513
[2] Awschalom D D, Bassett L C, Dzurak A S, Hu E L and Petta J R 2013 Quantum spintronics: engineering and manipulating atom-like spins in semiconductors *Science* **339** 1174
[3] Aharonovich I, Englund D and Toth M 2016 Solid-state single-photon emitters *Nat. Photon.* **10** 631
[4] Atatüre M, Englund D, Vamivakas N, Lee S-Y and Wrachtrup J 2018 Material platforms for spin-based photonic quantum technologies *Nat. Rev. Mater.* **3** 38
[5] Gao W B, Imamoglu A, Bernien H and Hanson R 2015 Coherent manipulation, measurement and entanglement of individual solid-state spins using optical fields *Nat. Photon.* **9** 363
[6] Hensen B *et al* 2015 Loophole-free Bell inequality violation using electron spins separated by 1.3 kilometres *Nature* **526** 682
[7] Sipahigil A, Jahnke K D, Rogers L J, Teraji T, Isoya J, Zibrov A S, Jelezko F and Lukin M D 2014 Indistinguishable photons from separated silicon-vacancy centers in diamond *Phys. Rev. Lett.* **113** 113602
[8] Klimov P V, Falk A L, Christle D J, Dobrovitski V V and Awschalom D D 2015 Quantum entanglement at ambient conditions in a macroscopic solid-state spin ensemble *Sci. Adv.* **1** e1501015
[9] Magnusson B and Janzén E 2005 Optical characterization of deep level defects in SiC *Mater. Sci. Forum* **483** 341
[10] Zargaleh S *et al* 2016 Evidence for near-infrared photoluminescence of nitrogen vacancy centers in 4h-SiC *Phys. Rev.* B **94** 060102
[11] Gällström A *et al* 2015 Optical properties and Zeeman spectroscopy of niobium in silicon carbide *Phys. Rev.* B **92** 075207
[12] Koehl W F, Diler B, Whiteley S J, Bourassa A, Son N T, Janzén E and Awschalom D D 2017 Resonant optical spectroscopy and coherent control of Cr^{4+} spin ensembles in SiC and GaN *Phys. Rev.* B **95** 035207
[13] Bosma T *et al* 2018 Identification and tunable optical coherent control of transition-metal spins in silicon carbide *npj Quantum Inf.* **4** 48
[14] Spindlberger L *et al* 2019 Optical properties of vanadium in 4H silicon carbide for quantum technology *Phys. Rev. Appl.* **12** 014015
[15] Csóré A and Gali A 2019 *Ab initio* determination of pseudospin for paramagnetic defects in SiC (arXiv:1909.11587)
[16] Wolfowicz G, Anderson C P, Diler B, Poluektov O G, Heremans F J and Awschalom D D 2020 Vanadium spin qubits as telecom quantum emitters in silicon carbide *Sci. Adv.* **6** eaaz1192
[17] Diler B, Whiteley S J, Anderson C P, Wolfowicz G, Wesson M E, Bielejec E S, Heremans F J and Awschalom D D 2020 Coherent control and high-fidelity readout of chromium ions in commercial silicon carbide *npj Quantum Inf.* **6** 11

[18] Baur J, Kunzer M and Schneider J 1997 Transition metals in SiC polytypes, as studied by magnetic resonance techniques *Phys. Status Solid a* **162** 153
[19] Kaufmann B, Dörnen A and Ham F S 1997 Crystal-field model of vanadium in 6H silicon carbide *Phys. Rev.* B **55** 13009
[20] Abragam A and Bleaney B 1970 *Electron Paramagnetic Resonance of Transition Ions* (*International Series of Monographs on Physics*) (Oxford: Clarendon)
[21] Tokura Y, van der Wiel W G, Obata T and Tarucha S 2006 Coherent single electron spin control in a slanting zeeman field *Phys. Rev. Lett.* **96** 047202
[22] Beaudoin F, Lachance-Quirion D, Coish W A and Pioro-Ladrière M 2016 Coupling a single electron spin to a microwave resonator: controlling transverse and longitudinal couplings *Nanotechnology* **27** 464003
[23] Kobayashi T *et al* 2020 Engineering long spin coherence times of spin–orbit qubits in silicon *Nat. Mater.* (https://doi.org/10.1038/s41563-020-0743-3)
[24] Khan M A, Erementchouk M, Hendrickson J and Leuenberger M N 2017 Electronic and optical properties of vacancy defects in single-layer transition metal dichalcogenides *Phys. Rev.* B **95** 245435
[25] Hepp C *et al* 2014 Electronic structure of the silicon vacancy color center in diamond *Phys. Rev. Lett.* **112** 036405
[26] Bradac C, Gao W, Forneris J, Trusheim M E and Aharonovich I 2019 Quantum nanophotonics with group IV defects in diamond *Nat. Commun.* **10** 5625
[27] Supplementary information available upon request.
[28] Beha K, Batalov A, Manson N B, Bratschitsch R and Leitenstorfer A 2012 Optimum photoluminescence excitation and recharging cycle of single nitrogen-vacancy centers in ultrapure diamond *Phys. Rev. Lett.* **109** 097404
[29] Wolfowicz G, Anderson C P, Yeats A L, Whiteley S J, Niklas J, Poluektov O G, Heremans F J and Awschalom D D 2017 Optical charge state control of spin defects in 4H-SiC *Nat. Commun.* **8** 1876
[30] Zwier O V, O'Shea D, Onur A R and van der Wal C H 2015 All–optical coherent population trapping with defect spin ensembles in silicon carbide *Sci. Rep.* **5** 10931
[31] Stevens K W H 1967 The theory of paramagnetic relaxation *Rep. Prog. Phys.* **30** 189
[32] Kiel A and Mims W B 1967 Paramagnetic relaxation measurements on Ce, Nd, and Yb in CaWO4by an electron spin-echo method *Phys. Rev.* **161** 386
[33] Shrivastava K N 1983 Theory of spin–lattice relaxation *Phys. Status Solid b* **117** 437
[34] Harris E A and Yngvesson K S 1968 Spin–lattice relaxation in some iridium salts I. Relaxation of the isolated (IrCl6)2- complex *J. Phys. C: Solid State Phys.* **1** 990
[35] Trusheim M E *et al* 2020 Transform-limited photons from a coherent tin-vacancy spin in diamond *Phys. Rev. Lett.* **124** 023602
[36] Thiering G and Gali A 2018 *Ab initio* magneto-optical spectrum of group-IV vacancy color centers in diamond *Phys. Rev.* X **8** 021063
[37] Jahnke K D, Sipahigil A, Binder J M, Doherty M W, Metsch M, Rogers L J, Manson N B, Lukin M D and Jelezko F 2015 Electron-phonon processes of the silicon-vacancy centre in diamond *New J. Phys.* **17** 043011
[38] Gällström A *et al* 2012 Optical identification and electronic configuration of tungsten in 4H- and 6H-SiC *Physica* B **407** 1462
[39] Kunzer M, Müller H D and Kaufmann U 1993 Magnetic circular dichroism and site-selective optically detected magnetic resonance of the deep amphoteric vanadium impurity in 6H-SiC *Phys. Rev.* B **48** 10846
[40] Dalibor T, Pensl G, Matsunami H, Kimoto T, Choyke W J, Schöner A and Nordell N 1997 Deep defect centers in silicon carbide monitored with deep level transient spectroscopy *Phys. Status Solid a* **162** 199